β-GALACTOSYLCERAMIDASE PROMOTES MELANOMA GROWTH VIA MODULATION OF CERAMIDE METABOLISM

Mirella Belleri[1], Giuseppe Paganini[1], Daniela Coltrini[1], Roberto Ronca[1], Daniela Zizioli[1], Michela Corsini[1], Andrea Barbieri[1], Elisabetta Grillo[1], Stefano Calza[1], Roberto Bresciani[1], Eugenio Maiorano[2], Mauro G. Mastropasqua[2], Tiziana Annese[3], Arianna Giacomini[1], Domenico Ribatti[3], Josefina Casas[4], Thierry Levade[5], Gemma Fabrias[4], Marco Presta[1,6§]

Affiliations:

[1]Department of Molecular and Translational Medicine, University of Brescia, Italy.
[2]Department of Emergency and Transplantation, Pathology Section, University of Bari Medical School, Bari, Italy.
[3]Department of Basic Medical Sciences, Neurosciences, and Sensory Organs, University of Bari Medical School, Bari, Italy.
[4]Research Unit on BioActive Molecules (RUBAM), Department of Biological Chemistry, Institute for Advanced Chemistry of Catalonia (IQAC), Spanish Council for Scientific Research (CSIC) Barcelona, and Liver and Digestive Diseases Networking Biomedical Research Centre (CIBER-EHD), Madrid, Spain.
[5]INSERM U1037, CRCT (Cancer Research Center of Toulouse) and Laboratoire de Biochimie Métabolique, Institut Fédératif de Biologie, CHU Purpan, Toulouse, France.
[6]Italian Consortium for Biotechnology (CIB), Unity of Brescia, Italy.

Correspondence to: Marco Presta (marco.presta@unibs.it) and Mirella Belleri (mirella.belleri@unibs.it), Department of Molecular and Translational Medicine, University of Brescia, viale Europa 11, 25123 Brescia, Italy.

Running title: β-galactosylceramidase in melanoma

Keywords: ceramide, galactosylceramidase, gene knockdown, lipid analysis, melanoma, mRNA in situ hybridization, sphingolipids, sphingomyelinase, zebrafish**.**

Financial support: This work was supported in part by Associazione Italiana per la Ricerca sul Cancro (AIRC) IG grant n° 18493 and MFAG grant n° 18459 to M.P. and R.R., respectively.

Conflict of interest: The authors declare no potential conflicts of interest

Text word count: 5000

Abstract word count: 249

Number of figures: 7

ABSTRACT

Disturbance of the sphingolipid metabolism may represent a novel therapeutic target in metastatic melanoma, the most lethal form of skin cancer. β-galactosylceramidase (GALC) removes β-galactose from galactosylceramide and other sphingolipids. This study stemmed from *in situ* hybridization and gene knockdown experiments showing that downregulation of *galcb*, a zebrafish orthologue of human *GALC*, affects melanoblast/melanocyte differentiation in zebrafish embryo, pointing to a possible role for GALC in melanoma. On this basis, the impact of GALC expression on murine B16-F10 and human A2058 melanoma cells was investigated following its silencing or upregulation. *Galc* knockdown hampers the growth, motility and invasive capacity of B16-F10 cells and their tumorigenic and metastatic activity when grafted in syngeneic mice or zebrafish embryos. *Galc*-silenced cells show alterations of the sphingolipid metabolism and an increase of the intracellular levels of ceramide, paralleled by a non-redundant upregulation of *Smpd3* that encodes for the ceramide-generating enzyme neutral sphingomyelinase 2. Accordingly, *GALC* downregulation causes *SMPD3* upregulation, increases ceramide levels and inhibits the tumorigenic activity of human melanoma A2058 cells whereas *GALC* upregulation exerts opposite effects. Finally, in keeping with information from melanoma database mining, RNAscope analysis demonstrates a progressive increase of *GALC* expression from common nevi to stage IV human melanoma samples that was paralleled by an increase of microphtalmia transcription factor and tyrosinase immunoreactivity and was inversely related to SMPD3 and ceramide levels. Our findings indicate that GALC may play an oncogenic role in melanoma by modulating the levels of intracellular ceramide, thus providing novel insights for melanoma therapy.

Statement of significance

Experiments performed on zebrafish embryos, murine and human melanoma cell lines and patient-derived tumor specimens indicate that β-galactosylceramidase plays an oncogenic role in melanoma, thus providing novel insights for melanoma therapy.

INTRODUCTION

Melanoma is a skin tumor that arises from neural crest-derived melanocytes (1). Resistant to chemotherapy and radiotherapy, metastatic melanoma represents the most lethal form of skin cancer (2). Thus, a more detailed understanding of melanocyte development and differentiation may provide valuable information about the mechanisms that contribute to melanoma progression and for the development of novel therapeutic options (3).

Sphingolipids regulate various biological processes in cancer (4). In particular, ceramide acts as a tumor suppressor and defects in ceramide generation and metabolism contribute to tumor cell survival and resistance to chemotherapy (5).

In melanoma, the expression of *acid sphingomyelinase*, which catalyzes the breakdown of sphingomyelin to ceramide and phosphocholine, affects melanoma cell proliferation, survival and dissemination and correlates inversely with tumor stage (6). In addition, downregulation of *sphingomyelin synthase 1*, which metabolizes ceramide into sphingomyelin, represents a worse prognosis biomarker in metastatic melanoma (7). Conversely, downregulation of the lactosylceramide synthase *β4-galactosyltransferase 5* suppresses the tumorigenic potential of murine melanoma cells (8) whereas *ceramide synthase 6* expression is related to the malignant behavior of human melanoma (9). Moreover, upregulation of neutral sphigomyelinase activity, with a subsequent increase of intracellular ceramide, elicits melanoma cell death (10). Together, these data indicate that disturbance of ceramide metabolism exerts a deep impact on melanoma and may represent a target for anticancer therapy.

β-Galactosylceramidase (GALC) (11) is a lysosomal hydrolase that catalyzes the removal of β-galactose from β-galactosylceramide and other sphingolipids, including galactosylsphingosine (psychosine). GALC deficiency causes globoid cell leukodystrophy (OMIM #245200), a sphingolipidosis characterized by degeneration of oligodendroglia and progressive demyelination (12). Two *GALC* co-orthologs (named *galca* and *galcb*) are co-expressed in zebrafish (*Danio rerio*) embryo (13). Both genes encode for lysosomal enzymes endowed with GALC activity and double *galca*/*galcb* knockdown provides evidence for a role of GALC activity in brain development in zebrafish (13).

Here, we found that *galcb* is transiently expressed by melanoblasts/melanocytes in zebrafish embryos and that its downregulation affects the differentiation of these cells. In keeping with the correlation observed among genes that regulate melanocyte development and those that contribute

to malignant melanoma (3, 14), we measured high levels of *Galc* expression in B16-F10 cells, a prototypic murine melanoma model. Notably, *Galc*-silenced B16-F10 cells showed a significant decrease in their tumorigenic and metastatic activity. This was paralleled by the accumulation of ceramide and upregulation of *sphingomyelin phosphodiesterase 3 (Smpd3)* that encodes for the ceramide-producing enzyme neutral sphingomyelinase 2. Consistent with these observations, modulation of *GALC* expression affected the tumorigenic activity of human melanoma A2058 cells. Accordingly, RNAscope analysis and tumor data mining revealed that the levels of *GALC* expression are related to human skin melanoma progression. Altogether, our observations show that GALC affects the tumorigenic activity of melanoma cells and may represent a novel target for melanoma therapy.

MATERIALS AND METHODS

Zebrafish maintenance. Wild-type AB, *casper* (15) and Tg(kdr:EGFP) (16) zebrafish lines were maintained at 28°C on a 14 h light/10 h dark cycle. After spawning, fertilized eggs were incubated at 28°C. Embryos were staged and maintained in 0.003% 1-phenyl-2-thiourea (Sigma) starting from 24 h post fertilization (hpf) unless specified otherwise. Zebrafish experiments were performed as approved by the local animal ethics committee (OPBA, Organismo Preposto al Benessere degli Animali, Università degli Studi di Brescia, Italy).

Whole mount *in situ* hybridizations (WISH). WISH was carried out on 4% paraformaldehyde-fixed zebrafish embryos (13). Digoxigenin-labeled RNA probes were transcribed from linear cDNA constructs and hybridizations were carried out overnight at 68°C (13). The expression of the genes under investigation following *galcb* knockdown was scored blindly as normal or downregulated by two independent observers and data were analyzed by the chi-squared test.

Morpholino (MO)-mediated *galcb* knockdown. Gene knockdown experiments were performed as described (13). Specific *galcb*-MO (5'-GCAGAGTTTACCTGTAGTCTG-3') targeting the exon 3 of zebrafish transcript was injected (1.4 pmol) into the yolk of 1–4-cell stage embryos. Std-MO (5'-CCTCTTACCTCAGTTACAATTTATA-3') was used as control. Sense mRNA encoding full length *galcb* was

transcribed *in vitro* from pGEM-T Easy/*galcb* vector using mMESSAGE mMACHINE kit and Poly(A) Tailing Kit (Ambion).

Cell cultures and lentivirus infection. B16-F10 and A2058 melanoma cells were obtained from ATCC-LGC Standards Repository (ATCC number CRL-6475 and CRL-2731, respectively), maintained at low passage and tested for Mycoplasma negativity. B16-F10 cell subcloning was performed as described in Supplemental Information. B16-F10 and A2058 cell silencing was carried out by transduction of lentiviral particles encoding mouse *Galc* or human *GALC* targeting short hairpin RNA, respectively. For GALC overexpression, A2058 cells were infected with a lentivirus harboring the murine *Galc* cDNA. See Supplemental Information for more details.

In vitro assays. *Cell proliferation.* B16-F10 cells were seeded at 10^4 cells/cm^2 in medium supplemented with 0.4% FBS. After 24 h (T_0), fresh medium was added and cells were counted 24-72 h thereafter. When described, cells were treated with GW4869 (Sigma-Aldrich; dissolved in ethanol) in medium containing 2.0% FBS and counted 24 h thereafter. A2058 cells were seeded in 24-well plates at 10^4 cells/cm^2 in medium added with 1.0% FBS. After 24 h (T_0), cells were added with fresh medium and counted 24 h and 48 h thereafter.

Colony formation. 500 or 5,000 cells were seeded in 35 mm-culture dishes or embedded in Matrigel (Cultrex BME, Gaithersburg, MD) and seeded in 24-well plates. After 15 days, cell colonies were observed under a phase contrast microscope and photographed.

Wound healing. Confluent B16-F10 cells were scraped with a 1000 µl tip to obtain a mechanical wound and maintained in Dulbecco's modified Eagle medium, supplemented with 0.4% FBS. Cells at the leading edge of the wound were observed by time-lapse microscopy as described in Supplemental Information.

Trans-endothelial migration. B16-F10 cells stained with CellTracker Red CMTPX Dye were seeded at 10^4 cells/well on a murine 1G11 endothelial cell monolayer stained with CellTracker Green CMFDA Dye (Thermo Fisher Scientific). Time-lapse microscopy was performed under an inverted Zeiss Axiovert 200 M photomicroscope (one snap photograph every 15 min) and the percentage of invading cells was calculated after 12 h.

GALC activity assay. GALC-mediated hydrolysis of the fluorescent GALC substrate LRh-6-GalCer (*N*-lissamine rhodaminyl-6-aminohexanoylgalactosyl ceramide) following its incubation with 30 µg of cell extract was quantified by thin-layer chromatography (TLC) (13).

Quantitative RT-PCR (RT-qPCR) analysis. B16-F10 cells were analysed by RT-qPCR using the primers listed in **Table S1** and data were normalized for *Gapdh* expression (17). See Supplemental Information for more details.

Lipid analysis. Lipids were extracted and analysed as previously described with minor modifications (18, 19). Separation of GlcCer and GalCer was attempted as reported by Nakajima et al. (20) with minor modifications.

Zebrafish embryo trans-endothelial migration assay. shNT-B16-F10 and shGALC-B16-F10 cells were stained with CellTracker Red CMTPX Dye or CellTracker Blue CMF2HC Dye (Thermo Fisher Scientific), respectively, and mixed at 1:1 ratio (5 x 10^3 cells/µl). Then, 4 nl containing 20 cells for each cell type were injected into the blood circulation of transgenic Tg(kdr:EGFP) zebrafish embryos at 48 hpf. Trans-endothelial migration in intersomitic vessels was evaluated at different h post-injection (hpi) (21).

Zebrafish embryo metastasis assay. B16-F10 cells were stained with CellTracker Green CMFDA Dye or CellTracker Red CMTPX Dye. Then, 80-100 cells/embryo were injected at 48 hpf into the blood circulation of wild-type AB or Tg(kdr:EGFP) zebrafish embryos, respectively. During the next 3 days, the growth of metastases in the tail vascular plexus was quantified by fluorescence microscopy followed by computerized image analysis (22).

Mice. C57BL/6 and NOD/Scid mice (Charles River, Calco, Italy) and breeder *twitcher* heterozygous mice (C57BL/6J, *twi/+*; Jackson Laboratories, ME) were maintained under standard conditions. Experiments were performed according to the Italian laws (D.L. 116/92 and following additions) that enforce the EU 86/109 Directive and were approved by the local animal ethics committee (OPBA, Università degli Studi di Brescia, Italy).

Tumorigenesis assay. C57BL/6 or NOD/Scid mice were injected subcutaneously (s.c.) into the dorsolateral flank with 3 x 10^4 B16-F10 cells or 3 x 10^6 A2058 cells, respectively, and tumors were measured with calipers. When indicated, tumors were harvested and processed for RT-qPCR analysis or GALC, SMPD3 and ceramide immunostaining as described in Supplemental Information.

Experimental lung metastasis assay. B16-F10 cells (5 x 10^4 cells in 100 µl of PBS) were injected into the tail vein of 7-week-old C57BL/6 mice. After 3 weeks, lungs were harvested and metastases were counted under a dissecting microscope.

RNAscope, immunohistochemistry (IHC) and morphometric analysis of human melanoma samples. Tissue samples from 60 patients who underwent curative resection were collected from the archive of the Unit of Pathology of the University of Bari, Hospital Policlinico, Bari, Italy. The study was approved by the Institutional Review Board at Hospital Policlinico (Bari) and conducted in accordance with GCP and the Declaration of Helsinki. Written informed consent was obtained from all patients. Tumors were divided into five histological subgroups: common nevi (n = 10), dysplastic nevi (n = 10), melanoma stages I-II (n = 20), melanoma stage III (n = 10), and melanoma stage IV (n = 10).
RNA in situ hybridization was performed using RNAscope® 2.5 HD Reagent Kit [RED 322360, Advanced Cell Diagnostics (ACD), Hayward, CA] using an Hs-GALC probe (ref. 566801), positive control probe Hs-PPIB (ref. 313901), or negative control probe DapB (ref. 310043). Immunohistochemistry was performed on the same 60 samples used for RNAscope analysis using mouse monoclonal anti-MITF (ref. M3621, Agilent Dako), anti-tyrosinase (ref. M3623, Agilent Dako), anti-SMPD3 (ref. sc-166637, Santa Cruz Biotechnology) and anti-ceramide (Enzo Life Science) antibodies. RNAscope measurements were defined as number of probes per cell nucleus. MITF, tyrosinase, SMPD3 and ceramide IHC staining were quantified by morphometric analysis. See Supplemental Information for more details.

RESULTS

GALC affects melanocyte differentiation in zebrafish.

The zebrafish genes *galca* and *galcb*, co-orthologs of human *GALC*, are co-expressed in embryonic brain during development (13). A detailed WISH analysis of *galca* and *galcb* expression in zebrafish

embryos at 28 and 40 hpf revealed that *galcb*, but not *galca*, is expressed also by melanoblasts/melanocytes alongside the embryo trunk (**Figure 1A**). No *galcb*-positive cells were instead detected along the trunk of *casper* zebrafish mutants that lack all melanophores (15), thus confirming the identity of these cells as melanoblasts/melanocytes (**Figure 1A**). Notably, *galcb* expression in embryonic melanocytes is transient, being lost at 48 hpf.

To assess the impact of *galcb* expression on zebrafish embryo melanocytes, loss-of-function studies were performed using a specific *galcb*-MO that induces skipping of exon 3 of the immature *galcb* mRNA, leading to the formation of an enzymatically inactive protein (13). When compared to controls, *galcb* morphants showed a significant delay in the appearance of melanin-positive melanocytes migrating laterally onto the yolk and dorsally to the embryo tail (**Figure 1B-C**). Co-injection of the *galcb*-MO with an excess of *galcb* mRNA fully rescued this defective phenotype (**Figure 1B-C**). No defects in melanocyte appearance were observed in embryos injected with an anti-*galca* MO (13) (**Figure S1A**), thus confirming the specificity of *galcb*-MO effects.

Zebrafish melanocytes develop from *crestin*-positive neural crest cells where the *SRY-related HMG-box 10* (*sox10*) transcription factor plays a primary role in pigment cell lineage fate specification. In melanoblasts, *sox10* activates the *microphtalmia transcription factor (mitfa*), involved in melanocyte differentiation. Finally, *dopachrome tautomerase* (*dct*) and *tyrosinase* (*tyr*) are markers of differentiating and terminally differentiated melanocytes, respectively (23). As shown in **Figure 1D-E**, *galcb* knockdown caused a significant inhibition ($P < 0.001$, Chi-squared test) of the expression of the melanoblast/melanocyte markers *mitfa*, *dct* and *tyr*, with no effect on *crestin* and *sox10* expression. No defects in *mitfa* and *dct* expression were instead observed in *galca* morphants (**Figure S1B**). These data point to a role for *galcb* in the differentiation, but not specification, of embryonic melanocytes in zebrafish.

GALC downregulation inhibits murine melanoma cell growth and motility.

An increasing evidence correlates genes that regulate melanocyte development with those that contribute to malignant melanoma (3, 14). These findings prompted us to assess *Galc* expression in B16-F10 cells, a prototypic murine melanoma model.

As shown in **Figure 2A**, B16-F10 cells express high levels of *Galc*, similar to those observed in the adult murine brain. Accordingly, a significant GALC activity was detected in B16-F10 cell extract and a

strong GALC immunoreactivity signal is present in B16-F10 tumor grafts when compared to the peritumoral tissue.

To assess the role of *Galc* in this melanoma model, B16-F10 cells were infected with lentiviral particles containing a shRNA target-specific construct designed to knockdown the *Galc* gene. The puromycin-resistant cell population (shGALC-B16-F10 cells) showed a significant GALC downregulation in terms of *Galc* transcript, protein levels and enzymatic activity when compared to cells infected with a non-targeting control shRNA (shNT-B16-F10 cells) (**Figure 2B**).

GALC downregulation caused the decrease in the growth rate of *Galc*-silenced cells when compared to shNT-B16-F10 and uninfected cells [cell duplication time (mean ± S.E.M.) equal to 32.3 ± 1.9 *versus* 17.5 ± 2.2 and 20.8 ± 1.5 h, respectively] (**Figure 2C**). Consistently, shGALC-B16-F10 cells showed a reduced colony formation capacity on tissue culture plastic or in a 3D Matrigel layer (**Figure 2D**). At variance, no differences in cell cycle distribution and apoptosis were observed among uninfected, shNT-B16-F10 and shGALC-B16-F10 cells (**Figure S2**).

To confirm the impact of *Galc* silencing on the growth capacity of B16-F10 cells, single cell-derived clones were obtained from shNT-B16-F10 and shGALC-B16-F10 cell populations. After single cell seeding, the days required by each clone to reach a number of cells equal to 5.0×10^6 was calculated. As shown in **Figure 2E,** only 16/28 shGALC-B16-F10 clones showed a rapid rate of growth when compared to 25/27 shNT-B16-F10 clones ($P < 0.01$, Chi-squared test). RT-qPCR analysis confirmed that the levels of *Galc* expression in shGALC-B16-F10 clones were lower than in shNT-B16-F10 clones. In addition, a significant inverse correlation was found between the levels of *Galc* expression in each clone and its proliferative capacity (**Figure 2F**).

Next, time-lapse videomicroscopy was used to assess the effect of *Galc* downregulation on the motility of B16-F10 cells in a mechanical wound healing assay. When compared to uninfected and shNT-B16-F10 cells, shGALC-B16-F10 cells showed a significant decrease in their capacity to repair the wounded cell monolayer with a reduction of their velocity and accumulated distance (**Figure 2G**). In addition, the capacity of B16-F10 cells to invade a murine microvascular endothelial cell monolayer was assessed *in vitro* (24). As shown in **Figure 2H**, shNT-B16-F10 cells adhere on the top of endothelial cells, cross the endothelium and attach to the substratum. This process was significantly impaired in shGALC-B16-F10 cells. For both cell populations, melanoma cell invasion was hampered by

neutralizing antibodies against N-cadherin, a major mediator of endothelium-melanoma cell adhesion (25).

GALC downregulation alters the sphingolipid profile of murine melanoma cells.

The sphingolipid, phospholipid and neutral lipid composition of B16-F10, shNT-B16-F10 and shGALC-B16-F10 cells was investigated. Among the sphingolipids tested (see **Table S2** for a complete list of all the analyzed lipids), shGALC-B16-F10 cells were characterized by a significant increase of the levels of ceramide (**Figure 3A**). This was paralleled by a decrease of sphingomyelins that occurred concomitantly to the reduction of phosphatidylethanolamines/lyso-phosphatidylethanolamines, cholesteryl esters and phosphatidylcholines, in parallel with an increased concentration of diacylglycerols (**Figure 3A**). At variance, no alterations of the levels of hexosyl- and lactosyl-ceramides, as well as of sphingosine-1-phosphate were observed following GALC downregulation. It must be mentioned that the separation of GalCer and GlcCer could not be achieved to background level. Since GlcCer is more abundant than GalCer, GlcCer levels may mask a possible difference in amounts of GalCer between control and *Galc*-silenced cells.

These findings prompted us to assess the levels of expression of a series of enzymes of the sphingolipid metabolism (**Figure 3B** and **Table S3**). In keeping with the observed alterations of the ceramide/sphingomyelin ratio, shGALC-B16-F10 cells displayed a remarkable upregulation of *Smpd3* expression. *Smpd3* encodes for neutral sphingomyelinase 2 that catalyzes the hydrolysis of sphingomyelin to ceramide and phosphocholine. No alteration was observed for the expression levels of the acid lysosomal sphingomyelinase *Smpd1*, as well as of all the other enzymes tested.

Twitcher mice are characterized by a spontaneous *Galc* mutation that results in a dramatic reduction of GALC activity in homozygous *twi/twi* animals (26). In accordance with the results obtained for shGALC-B16-F10 cells, a significant *Smpd3* upregulation was observed in post-natal fibroblasts, lung, liver and kidney of *twi/twi* mice when compared to wild type animals (**Figure 3C**), thus supporting the hypothesis that of an inverse correlation may exist between *Galc* downregulation and *Smpd3* upregulation.

In order to assess whether *Smpd3* upregulation may contribute to the oncosuppressive activity exerted by *Galc* downregulation, shGALC-B16-F10 and shNT-B16-F10 cells were treated with the neutral sphingomyelinase inhibitor GW4869 (27). As shown in **Figure 3D-E**, GW4869 caused a

significant stimulation of shGALC-B16-F10 cell proliferation paralleled by a decrease of intracellular ceramide content, with no effect on the proliferation of shNT-B16-F10 cells. Together, these data point to a role for *Smpd3* upregulation, with a consequent increase of ceramide content, in mediating the inhibitory effect exerted by *Galc* silencing in B16-F10 cells.

GALC downregulation inhibits the tumorigenic and metastatic activity of murine melanoma cells.

To evaluate the impact of *Galc* downregulation on the tumorigenic activity of B16-F10 cells, shNT-B16-F10 and shGALC-B16-F10 cells were implanted subcutaneously in syngeneic C57BL/6 mice. As shown in **Figure 4A**, *Galc* downregulation caused a significant delay in shGALC-B16-F10 tumor growth when compared to shNT-B16-F10 lesions. Accordingly, the average weight of shGALC-B16-F10 tumors harvested 26 days after grafting was significantly smaller than that of shNT-B16-F10 lesions that expressed higher levels of *Galc* transcript and of the cell proliferation marker *Cyclin D1* (**Figure 4A**). In keeping with the *in vitro* observations, immunohistochemical analysis showed an increase of SMPD3 protein levels in shGALC-B16-F10 tumors when compared to controls, which was paralleled by a significant increase of ceramide levels (**Figure 4B**). At variance, shGALC-B16-F10 and shNT-B16-F10 grafts did not differ in the expression levels of various immune checkpoint genes and tumor cell infiltrate markers (including monocyte/macrophage, B and T lymphocyte, NK cell and granulocyte markers) (**Table S4**). Notably, consistent with *in vitro* data, *in vivo* administration of the neutral sphingomyelinase inhibitor GW4869 increased the rate of growth of shGALC-B16-F10 tumor grafts, further supporting the role of neutral sphingomyelinase activity in mediating the anti-tumorigenic effects exerted by *Galc* downregulation in B16-F10 melanoma cells (**Figure S3**).

In a second set of experiments, shNT-B16-F10 and shGALC-B16-F10 cells were injected into the tail vein of C57BL/6 mice and experimental lung metastases were counted 3 weeks after. As illustrated in **Figure 4C**, *Galc* downregulation caused a significant decrease in the metastatic potential of melanoma cells when compared to controls.

Tumor cell extravasation represents an important step in the metastatic process. To assess whether *Galc* downregulation affects the capacity of B16-F10 cells to extravasate in an *in vivo* zebrafish embryo model (21), shNT-B16-F10 and shGALC-B16-F10 were stained with the red fluorescent CellTracker Red CMTPX Dye and the blue fluorescent CellTracker Blue CMF2HC Dye, respectively. Then, cells were co-injected in the blood circulation of transgenic Tg(kdr:EGFP) zebrafish

embryos and the number of cells that migrated across the fluorescent EGFP positive-endothelium of intersomitic vessels was counted at different hpi (21). In keeping with *in vitro* data, blue fluorescent shGALC-B16-F10 cells showed a reduced ability to extravasate when compared to red fluorescent, control shNT-B16-F10 cells **(Figure 4D)**. On this basis, CellTracker Red CMTPX Dye-stained B16-F10 cells were injected into the blood stream of Tg(kdr:EGFP) zebrafish embryos at 48 hpf and the growth of micrometastases in the haematopoietic tissue of embryo tail was evaluated (22). As shown in **Figure 4E**, metastatic lesions generated by shGALC-B16-F10 cells showed a reduced rate of growth when compared to shNT-B16-F10 lesions.

To confirm these findings and in order to rule out possible off target effects of the anti-*Galc* shRNA used to generate shGALC-B16-F10 cells, we performed a second infection of B16-F10 cells with a lentivirus harboring a different anti-*Galc* shRNA, generating a novel, independent shGALC-B16-F10 cell population (shGALC-bis-B16-F10 cells). As observed for shGALC-B16-F10 cells, *Galc* downregulation caused a significant decrease of the proliferation, colony formation and motility of shGALC-bis-B16-F10 cells (**Figure S4A-D**). This resulted in a significant decrease of the tumorigenic and metastatic activity of these cells that was paralleled by an increase of SMPD3 and ceramide levels in shGALC-bis-B16-F10 tumor xenografts when compared to controls (**Figure S4E-H**). Collectively, these data demonstrate that *Galc* downregulation significantly hampers the tumorigenic activity of murine B16-F10 cells.

GALC affects the tumorigenic activity of human melanoma cells.

To further assess the impact of GALC expression in melanoma, human melanoma A2058 cells harboring the V600E B-RAF mutation (28) were infected with lentiviral particles containing a shRNA target-specific construct designed to knockdown the human *GALC* gene or a non-targeting control shRNA, thus generating shGALC-A2058 and shNT-A2058 cells, respectively. This resulted in a significant decrease of GALC activity in shGALC-A2058 cells when compared to controls (**Figure 5A**). In parallel, a second aliquot of A2058 cells was infected with a lentivirus harboring the murine *Galc* cDNA, thus generating upGALC-A2058 cells that exhibited a higher GALC activity when compared to A2058 cells transduced with an empty vector (mock-A2058 cells) (**Figure 5A**).

Again, an inverse correlation was observed between *GALC* and *SMPD3* expression in these A2058 cell populations (**Figure 5B**). In addition, upGALC-A2058 cells showed a higher proliferative capacity *in*

vitro or when grafted in NOD/Scid mice, whereas GALC down-regulation resulted in a decreased rate of growth of shGALC-A2058 cells both *in vitro* and *in vivo* (**Figure 5C-D**). Again, ceramide and SMPD3 protein levels in tumor grafts were inversely related to *GALC* expression in the different A2058 cell populations (**Figure 5E**).

In keeping with a pro-tumorigenic role of GALC in melanoma, Human Protein Atlas (www.proteinatlas.org) and Gene Expression Omnibus (https://www.ncbi.nlm.nih.gov/geo) data mining indicates that *GALC* expression levels in human tumor specimens are related to melanoma progression (**Figure S5A-B**). To confirm these observations, RNAscope analysis was performed on 60 human melanoma samples to evaluate *GALC* expression at different stages of tumor progression. In keeping with public data sets, morphometric analysis demonstrates a progressive increase of *GALC* expression starting from common nevi to stage IV melanomas that was paralleled by a progressive increase of MITF and tyrosinase immunoreactivity in the same samples (**Figure 6A-B**). Independently of tumor stage, a direct correlation was observed between *GALC* expression levels and MITF and tyrosinase immunoreactivity (**Figure 6C**). Similar results were obtained by the analysis of the gene expression levels of *GALC*, *MITF* and *TYR* in 103 human primary melanoma samples downloaded from the TCGA GDC Data Portal (**Figure S5C**). Finally, a progressive decrease of SMPD3 and ceramide immunoreactivity occurs in the human skin melanoma samples investigated starting from common nevi to stage IV melanomas (**Figure 7A-B**). Remarkably, both SMPD3 and ceramide immunoreactivity levels were inversely correlated to *GALC* expression in these samples, ceramide levels decreasing as a function of the *GALC* mRNA/SMPD3 protein ratio (**Figure 7C**). Accordingly, public data mining indicates that an inverse correlation might indeed exist between *GALC* and *SMPD3* mRNA levels in human melanoma and that *SMPD3* expression appears to be higher in human primary tumors when compared to melanoma metastases (**Figure S6A-C**).

DISCUSSION

Alterations in the metabolism of sphingolipids, including the tumor suppressor ceramide, exert a deep impact in melanoma (6-10). GALC catalyzes the removal of galactose from terminal β-galactose-containing sphingolipids (12). The present work demonstrates that GALC critically modulates the oncogenic activity of melanoma cells *in vitro* and *in vivo*.

Our study stemmed from the observation that *galcb*, the zebrafish orthologue of human *GALC* (13), is transiently expressed in melanoblasts/melanocytes of zebrafish embryo and that its downregulation affects melanocyte differentiation in zebrafish embryos. In keeping with the correlation observed among genes that regulate melanocyte development with those that contribute to malignant melanoma (3, 14), we found that *Galc* is highly expressed in murine B16-F10 melanoma cells. Enzyme knockdown by small interfering *Galc*-targeting shRNA resulted in a significant decrease of the proliferative, migratory, and invasive capacity of shGALC-B16-F10, paralleled by a reduced tumorigenic and metastatic activity *in vivo*. To rule out the possibility of off target effects, these findings were confirmed by a second infection of B16-F10 cells with a lentivirus harboring a different anti-*Galc* shRNA, generating a novel, independent shGALC-bis-B16-F10 cell population that showed a similar decrease in its tumorigenic and metastatic potential *in vitro* and *in vivo*. Similar results were observed following *GALC* silencing in human melanoma A2058 cells whereas *GALC* upregulation conferred a more potent tumorigenic activity to these cells.

In keeping with the hypothesis that GALC may exert a pro-oncogenic activity in melanoma, cancer data mining indicates that *GALC* expression in human tumor specimens is related to skin melanoma progression. Accordingly, RNAscope analysis performed at different stages of human melanoma progression demonstrates a progressive and significant increase of *GALC* expression starting from common nevi to stage IV melanoma.

Knockdown of *galcb* in zebrafish embryos causes the downregulation of genes involved in melanocyte differentiation, including *mitfa* and *tyr*. MITF plays an important role also in human melanoma progression by modulating tumor cell proliferation, survival and metastatic capacity (29, 30). Highly variable MITF expression levels are found in melanoma cell subpopulations that confer tumor heterogeneity and plasticity (31). In addition, peripheral blood *TYR* mRNA and tissue tyrosinase immunoreactivity are melanoma biomarkers (32, 33). Here we show that *GALC* expression correlates with MITF and tyrosinase immunoreactivity in a cohort of 60 human samples at different stages of melanoma progression. Accordingly, TCGA GDC Data Portal mining indicates that a direct correlation exists between *GALC* and *MITF*/*TYR* expression levels in a cohort of 103 human primary melanoma samples. Altogether, these data strongly argue for a role of GALC in human melanoma progression.

Genetic GALC deficiency causes globoid cell leukodystrophy (12), a neurodegenerative disease characterized by the accumulation of the cytotoxic sphingolipid metabolite psychosine (34). On the

other hand, experimental evidence indicates that GALC downregulation may exert also psychosine-independent effects. For instance, an altered expression of the neuronal marker *neuroD* and increased apoptotic events are observed in double *galca*/*galcb* zebrafish embryo morphants in the absence of any significant accumulation of psychosine (13). Similarly, *GALC* downregulation causes a significant decrease in the mitogenic and motogenic responses of human endothelial cells to vascular endothelial growth factor with only minor modifications in intracellular psychosine levels (35). These results raise the possibility that changes in sphingolipid metabolism, other than psychosine accumulation, may explain the biological effects consequent to the modulation of GALC activity. For instance, *Galc*-null *twitcher* mice show a significant increase in the brain levels of the GALC substrate lactosyl-ceramide (36), a lipid raft component implicated in signaling events linked to cell differentiation, development, apoptosis, and oncogenesis (37). In addition, *Galc* silencing affects the sphingolipid profile and functionality of murine hematopoietic stem cells (38).

Here, we demonstrate that *Galc* silencing deeply affects the sphingolipid, phospholipid and neutral lipid profiles of melanoma B16-F10 cells causing a significant increase of intracellular ceramide. This was accompanied by a decrease in sphingomyelin, with no alterations of hexosyl- and lactosyl-ceramides. Various sphingolipid metabolizing enzymes, including acid sphingomyelinase (6), the lactosyl-ceramide synthase β4-galactosyltransferase 5 (8) and ceramide synthase 6 (9), modulate ceramide levels and affect the malignant behavior of melanoma cells. Our results indicate that alterations of the ceramide/sphingomyelin balance that occur in shGALC-B16-F10 cells is accompanied by the upregulation of the neutral sphingomyelinase *Smpd3*, an enzyme that hydrolyzes sphingomyelin to ceramide, with a consequent increase of SMPD3 and ceramide levels in the corresponding tumor grafts. *Smpd3* upregulation was observed also in post-natal fibroblasts and different organs of *Galc*-null *twitcher* animals, pointing to an inverse correlation between *Galc* down-modulation and *Smpd3* upregulation.

Experimental evidence points to *SMPD3* as an oncosuppressor gene, neutral sphingomyelinase activity regulating tumor cell proliferation, survival and response to chemotherapy (39). Accordingly, increased neutral sphingomyelinase activity, with a consequent increase of intracellular ceramide generation, affects melanoma cell survival (10). Our data demonstrate that an inverse correlation exists between *GALC* and *SMPD3* expression also in human A2058 cells following *GALC* downregulation. In addition, we observed a progressive decrease of SMPD3 levels in human tumor

specimens starting from common nevi to stage IV melanoma. This was paralleled by the reduction of ceramide immunoreactivity in the same lesions, ceramide levels decreasing as a function of the *GALC* mRNA/SMPD3 ratio. In keeping with these observations, public data mining revealed an inverse correlation between *GALC* and *SMPD3* expression levels in human melanoma and a higher *SMPD3* expression in human primary tumors when compared to melanoma metastases. In addition, our data demonstrate that the neutral sphingomyelinase inhibitor GW4869 (27) causes a significant stimulation of the tumorigenic activity of shGALC-B16-F10 cells paralleled by a decrease of intracellular ceramide levels. Together, these data point to a role for *Smpd3* upregulation, with a subsequent increase of intracellular ceramide, in mediating the inhibitory effect exerted by *Galc* downregulation in melanoma.

Different chemotherapeutics can regulate *SMPD3* expression at the transcriptional levels *via* activation of Sp1 and Sp3 transcription factors (40). *SMPD3* upregulations occurs in response to several activators, including TNFα [(41) and references therein]. In addition, *SMPD3* has been identified as a p53 target gene downstream of the DNA damage pathway (42). Further experiments will be required to elucidate the molecular determinants of the inverse correlation existing between *GALC* and *SMPD3* expression in melanoma cells.

Beside the observed increase in ceramide levels, we cannot rule out the possibility that other alterations of the lipid profile following *Galc* silencing may contribute to the decreased oncogenic potential of melanoma cells. For instance, the increased levels of diacylglycerols measured in shGALC-B16-F10 cells may cause the downregulation of the novel protein kinase PKCε and PKCδ (43), both involved in the oncogenic behavior of melanoma cells *via* activation of the activating transcription factor 2 (44, 45) or suppression of caspase-dependent apoptosis in NRAS/BRAF mutated cells (46), respectively. Interestingly, recent observations have shown that SMPD3 deficiency disrupts the homeostasis of diacylglycerol, ceramide and sphingomyelin in the Golgi compartment (47). Comprehensive lipidomic profiling may provide relevant information about the tumorigenic/metastatic potential of melanoma cells (48). In this frame, our findings set the basis for further investigations aimed at assessing the relationship between defined lipid changes and *GALC* expression levels and their impact on melanoma.

In summary, GALC appears to play a non-redundant role in melanoma progression by affecting the tumorigenic and metastatic potential of melanoma cells due to its impact on their sphingolipid

metabolism. These observations indicate that GALC may represent a novel target for melanoma therapy.

REFERENCES

1. Miller AJ, Mihm MC, Jr. Melanoma. N Engl J Med 2006;355:51-65.
2. Garbe C, Peris K, Hauschild A, Saiag P, Middleton M, Spatz A, et al. Diagnosis and treatment of melanoma: European consensus-based interdisciplinary guideline. Eur J Cancer 2010;46:270-83.
3. Mort RL, Jackson IJ, Patton EE. The melanocyte lineage in development and disease. Development 2015;142:620-32.
4. Ogretmen B. Sphingolipid metabolism in cancer signalling and therapy. Nat Rev Cancer 2018;18:33-50.
5. Morad SA, Cabot MC. Ceramide-orchestrated signalling in cancer cells. Nat Rev Cancer 2013;13:51-65.
6. Bizzozero L, Cazzato D, Cervia D, Assi E, Simbari F, Pagni F, et al. Acid sphingomyelinase determines melanoma progression and metastatic behaviour via the microphtalmia-associated transcription factor signalling pathway. Cell Death Differ 2014;21:507-20.
7. Bilal F, Montfort A, Gilhodes J, Garcia V, Riond J, Carpentier S, et al. Sphingomyelin Synthase 1 (SMS1) Downregulation Is Associated With Sphingolipid Reprogramming and a Worse Prognosis in Melanoma. Front Pharmacol 2019;10:443.
8. Shirane K, Kuji R, Tareyanagi C, Sato T, Kobayashi Y, Furukawa S, et al. Gene expression levels of beta4-galactosyltransferase 5 correlate with the tumorigenic potentials of B16-F10 mouse melanoma cells. Glycobiology 2014;24:532-41.
9. Tang Y, Cao K, Wang Q, Chen J, Liu R, Wang S, et al. Silencing of CerS6 increases the invasion and glycolysis of melanoma WM35, WM451 and SK28 cell lines via increased GLUT1-induced downregulation of WNT5A. Oncol Rep 2016;35:2907-15.
10. Ferrer P, Asensi M, Priego S, Benlloch M, Mena S, Ortega A, et al. Nitric oxide mediates natural polyphenol-induced Bcl-2 down-regulation and activation of cell death in metastatic B16 melanoma. J Biol Chem 2007;282:2880-90.
11. Suzuki K, Suzuki Y. Globoid cell leucodystrophy (Krabbe's disease): deficiency of galactocerebroside beta-galactosidase. Proc Natl Acad Sci U S A 1970;66:302-9.

12. Won JS, Singh AK, Singh I. Biochemical, cell biological, pathological, and therapeutic aspects of Krabbe's disease. J Neurosci Res 2016;94:990-1006.
13. Zizioli D, Guarienti M, Tobia C, Gariano G, Borsani G, Bresciani R, et al. Molecular cloning and knockdown of galactocerebrosidase in zebrafish: new insights into the pathogenesis of Krabbe's disease. Biochim Biophys Acta 2014;1842:665-75.
14. White RM, Zon LI. Melanocytes in development, regeneration, and cancer. Cell Stem Cell 2008;3:242-52.
15. White RM, Sessa A, Burke C, Bowman T, LeBlanc J, Ceol C, et al. Transparent adult zebrafish as a tool for in vivo transplantation analysis. Cell Stem Cell 2008;2:183-9.
16. Choi J, Dong L, Ahn J, Dao D, Hammerschmidt M, Chen JN. FoxH1 negatively modulates flk1 gene expression and vascular formation in zebrafish. Dev Biol 2007;304:735-44.
17. Coltrini D, Di Salle E, Ronca R, Belleri M, Testini C, Presta M. Matrigel plug assay: evaluation of the angiogenic response by reverse transcription-quantitative PCR. Angiogenesis 2013;16:469-77.
18. Cingolani F, Casasampere M, Sanllehi P, Casas J, Bujons J, Fabrias G. Inhibiton of dihydroceramide desaturase activity by the sphingosine kinase inhibitor SKI II. J Lipid Res 2014;55:1711-20.
19. Simbari F, McCaskill J, Coakley G, Millar M, Maizels RM, Fabriás G, et al. Plasmalogen enrichment in exosomes secreted by a nematode parasite versus those derived from its mouse host: implications for exosome stability and biology. J Extracell Vesicles 2016;5:30741.
20. Nakajima K, Akiyama H, Tanaka K, Kohyama-Koganeya A, Greimel P, Hirabayashi Y. Separation and analysis of mono-glucosylated lipids in brain and skin by hydrophilic interaction chromatography based on carbohydrate and lipid moiety. J Chromatogr B Analyt Technol Biomed Life Sci 2016;1031:146-53.
21. Stoletov K, Kato H, Zardouzian E, Kelber J, Yang J, Shattil S, et al. Visualizing extravasation dynamics of metastatic tumor cells. J Cell Sci 2010;123:2332-41.
22. Tobia C, Gariano G, De Sena G, Presta M. Zebrafish embryo as a tool to study tumor/endothelial cell cross-talk. Biochim Biophys Acta 2013;1832:1371-7.
23. Ceol CJ, Houvras Y, White RM, Zon LI. Melanoma biology and the promise of zebrafish. Zebrafish 2008;5:247-55.

24. Ronca R, Di Salle E, Giacomini A, Leali D, Alessi P, Coltrini D, et al. Long pentraxin-3 inhibits epithelial-mesenchymal transition in melanoma cells. Mol Cancer Ther 2013;12:2760-71.
25. Conacci-Sorrell M, Zhurinsky J, Ben-Ze'ev A. The cadherin-catenin adhesion system in signaling and cancer. J Clin Invest 2002;109:987-91.
26. Suzuki K. The twitcher mouse: a model for Krabbe disease and for experimental therapies. Brain Pathol 1995;5:249-58.
27. Luberto C, Hassler DF, Signorelli P, Okamoto Y, Sawai H, Boros E, et al. Inhibition of tumor necrosis factor-induced cell death in MCF7 by a novel inhibitor of neutral sphingomyelinase. J Biol Chem 2002;277:41128-39.
28. Rozenberg GI, Monahan KB, Torrice C, Bear JE, Sharpless NE. Metastasis in an orthotopic murine model of melanoma is independent of RAS/RAF mutation. Melanoma Res 2010;20:361-71.
29. Vachtenheim J, Ondrusova L. Microphthalmia-associated transcription factor expression levels in melanoma cells contribute to cell invasion and proliferation. Exp Dermatol 2015;24:481-4.
30. Simmons JL, Pierce CJ, Al-Ejeh F, Boyle GM. MITF and BRN2 contribute to metastatic growth after dissemination of melanoma. Sci Rep 2017;7:10909.
31. Levy C, Khaled M, Fisher DE. MITF: master regulator of melanocyte development and melanoma oncogene. Trends Mol Med 2006;12:406-14.
32. Ordonez NG. Value of melanocytic-associated immunohistochemical markers in the diagnosis of malignant melanoma: a review and update. Hum Pathol 2014;45:191-205.
33. Tandler N, Mosch B, Pietzsch J. Protein and non-protein biomarkers in melanoma: a critical update. Amino Acids 2012;43:2203-30.
34. Suzuki K. Twenty five years of the "psychosine hypothesis": a personal perspective of its history and present status. Neurochem Res 1998;23:251-9.
35. Belleri M, Ronca R, Coltrini D, Nico B, Ribatti D, Poliani PL, et al. Inhibition of angiogenesis by beta-galactosylceramidase deficiency in globoid cell leukodystrophy. Brain 2013;136:2859-75.
36. Tominaga K, Matsuda J, Kido M, Naito E, Yokota I, Toida K, et al. Genetic background markedly influences vulnerability of the hippocampal neuronal organization in the "twitcher" mouse model of globoid cell leukodystrophy. J Neurosci Res 2004;77:507-16.

37. Chatterjee S, Pandey A. The Yin and Yang of lactosylceramide metabolism: implications in cell function. Biochim Biophys Acta 2008;1780:370-82.

38. Visigalli I, Ungari S, Martino S, Park H, Cesani M, Gentner B, et al. The galactocerebrosidase enzyme contributes to the maintenance of a functional hematopoietic stem cell niche. Blood 2010;116:1857-66.

39. Clarke CJ. Neutral sphingomyelinases in cancer: friend or foe? Adv Carcer Res 2018;140:97-119.

40. Ito H, Murakami M, Furuhata A, Gao S, Yoshida K, Sobue S, et al. Transcriptional regulation of neutral sphingomyelinase 2 gene expression of a human breast cancer cell line, MCF-7, induced by the anti-cancer drug, daunorubicin. Biochim Biophys Acta 2009;1789:681–690.

41. Shamseddine AA, Airola MV, Hannun YA. Roles and regulation of neutral sphingomyelinase-2 in cellular and pathological processes. Adv Biol Regul 2015;57:24-41.

42. Shamseddine AA, Clarke CJ, Carroll B, Airola MV, Mohammed S, Rella A, et al. P53-dependent upregulation of neutral sphingomyelinase-2: role in doxorubicin-induced growth arrest. Cell Death Dis 2015;6:e1947.

43. Lum MA, Barger CJ, Hsu AH, Leontieva OV, Black AR, Black JD. Protein kinase Cα (PKCα) Is resistant to long term desensitization/down-regulation by prolonged diacylglycerol stimulation. J Biol Chem 2016;291:6331-46.

44. Lau E, Feng Y, Claps G, Fukuda MN, Perlina A, Donn D, et al. The transcription factor ATF2 promotes melanoma metastasis by suppressing protein fucosylation. Sci Signal 2015;8:ra124.

45. Lau E, Kluger H, Varsano T, Lee K, Scheffler I, Rimm DL, et al. PKCepsilon promotes oncogenic functions of ATF2 in the nucleus while blocking its apoptotic function at mitochondria. Cell 2012;148:543-55.

46. Takashima A, English B, Chen Z, Cao J, Cui R, Williams RM, et al. Protein kinase Cdelta is a therapeutic target in malignant melanoma with NRAS mutation. ACS Chem Biol 2014;9:1003-14.

47. Stoffel W, Hammels I, Jenke B, Binczek E, Schmidt-Soltau I, Brodesser S, et al. Neutral sphingomyelinase (SMPD3) deficiency disrupts the Golgi secretory pathway and causes growth inhibition. Cell Death Dis 2016;7:e2488.

48. Kim HY, Lee H, Kim SH, Jin H, Bae J, Choi HK. Discovery of potential biomarkers in human melanoma cells with different metastatic potential by metabolic and lipidomic profiling. Sci Rep 2017;7:8864.

AUTHOR CONTRIBUTIONS

MB performed the experiments, analyzed the data and revised the paper. MC, EG, AG and RB performed in vitro experiments. DC performed RT-qPCR analysis. RR analyzed the data and performed in vivo experiments. GP, DZ and AB performed zebrafish experiments. SC performed bioinformatics analysis. EM and MGM collected clinical samples. TA performed RNAScope experiments and morphometric analysis. DM performed immunohistochemical analysis of clinical samples. JC and GF performed lipid analysis. TL revised the paper. MP conceived the study and wrote the paper

LEGENDS TO FIGURES

Figure 1. *Galcb* modulates melanocyte differentiation in zebrafish. **A,** WISH analysis demonstrates that *galcb*, but not *galca*, is expressed by melanoblasts/melanocytes in wild-type AB zebrafish embryos. No *galcb*-positive cells are detectable in *casper* zebrafish mutants that lack all melanophores. h, hindbrain; m, midbrain; mhb, midbrain–hindbrain boundary. **B,** Downregulation of *galcb* expression by *galcb*-MO injection decrease the number of melanin-positive melanocytes migrating over the yolk (red symbols) and the trunk (blue symbols) of zebrafish morphants when compared to control Std-MO injected embryos. The phenotype was fully rescued by co-injection of an excess of *galcb* mRNA. Data are the mean ± SEM, n = 60, * $P < 0.05$, ** $P < 0.01$. **C,** Representative images of embryos at 36 hpf. **D,** Galcb downregulation inhibits the expression of the melanoblast/melanocyte markers *mitfa*, *dct* and *tyr* with no effect on the earlier genes *crestin* and *sox10*. Embryos were scored blindly by two independent observers for a normal or downregulated expression of the gene under investigation. Data are shown as percentage of the indicated embryos. *** $P < 0.001$. **E,** Representative images of Std-MO and *galcb*-MO morphants showing a normal (black border) or downregulated (red border) expression of the gene under investigation.

Figure 2. *Galc* expression affects the proliferative and migratory potential of melanoma B16-F10 cells. **A,** RT-PCR (upper panel), enzymatic assay (middle panel) and immunostaining (lower panel) show the expression of *Galc* in melanoma B16-F10 cells. Scale bar: 100 μm. **B,** Western blot analysis (WB), enzymatic activity TLC assay and RT-qPCR analysis show GALC downregulation in lentivirus-infected shGALC-B16-F10 cells when compared to control cell populations. n = 6. **C-D,** *Galc* downregulation inhibits the growth and colony formation capacity of B16-F10 cells. **E,** Growth of single cell-derived shNT-B16-F10 and shGALC-B16-F10 clones (27 and 28 clones, respectively). The clones reaching the number of 5.0×10^6 cells/clone 30 days before or after seeding are marked by black or open bars, respectively. **F,** *Galc* expression levels of the clones originated from the shNT-B16-F10 and shGALC-B16-F10 populations are shown in the upper panel. A linear correlation exists between *Galc* mRNA levels of each clone and its rate of growth, defined as the number of days required to reach a number of cells equal to 5.0×10^6 cells/clone after initial single cell seeding (lower panel). **G,** Time-lapse

microscopy demonstrates that *Galc* downregulation inhibits the migratory capacity of B16-F10 cells after a mechanical scratch *in vitro* characterized by decreased accumulated distance and velocity. Representative images and tracking plots of shNT-B16-F10 and shGALC-B16-F10 cell monolayers are shown 8 h after wounding (red line) in left panels. Scale bar, 100 μm. **H,** *Galc* downregulation inhibits the invasive capacity of red fluorescent B16-F10 cells seeded on a monolayer of green fluorescent endothelial cells. An anti-N-cadherin antibody was used as control inhibitor. *Inset*: Red B16-F10 cells invading (asterisks) and non-invading (arrowheads) the green endothelial cell monolayer were photographed 12 h after seeding. Data are the mean ± SEM, ** $P < 0.01$.

Figure 3. *Galc* downregulation alters the sphingolipid profile of melanoma B16-F10 cells. **A,** Lipid quantification of uninfected, shNT-B16-F10 and shGALC-B16-F10 cell extracts. Cer, ceramides; SM, sphingomyelins; HexCer, monohexosylceramides; DAG, diacylglycerols; Chol.Est., cholesteryl esters; lyso-PEA, lyso-phosphatidylethanolamines; PEA, phosphatidylethanolamines; PC, phosphatidylcholines. **B,** *Galc* downregulation in B16-F10 cells is accompanied by the upregulation of the expression of neutral sphingomyelinase 2 (*Smpd3*). *Smpd1*, acid lysosomal sphingomyelinase; *Sgms1*, sphingomyelin synthase 1; *Sgms2*, sphingomyelin synthase 2; *Gba1*, acid β-glucosylceramidase; *Asah1*, acid ceramidase; *Cerk*, ceramide kinase; *Sphk1*, sphingosine kinase 1. **C,** *Smpd3* expression is increased in postnatal fibroblasts and different organs of twi/twi mice when compared to wild type animals. **D-E,** The neutral sphingomyelinase inhibitor GW4869 (5.0 μM) restores the proliferative capacity of shGALC-B16-F10 cells by decreasing the intracellular levels of ceramides. Data are the mean ± SEM of 3-5 determinations, * $P<0.05$*, * $P<0.01$**.

Figure 4. Reduced tumorigenic and metastatic activity of *Galc*-silenced melanoma B16-F10 cells. **A,** *Galc* downregulation inhibits the growth of B16-F10 xenografts injected s.c. in C57BL/6 mice (6 mice/group). shGALC-B16-F10 tumors show a reduced weight and lower levels of *Galc* and *Cyclin D1* expression when compared to control shNT-B16-F10 lesions. Similar results were obtained in three independent experiments. **B,** Immunohistochemical (ICH) analysis of SMPD3 and ceramide immunoreactivity in shNT-B16-F10 (n = 4) and shGALC-B16-F10 (n = 5) tumor grafts. Scale bar: 60 μm. **C,** shGALC-B16-F10 cells show a reduced lung metastatic activity when injected into the tail vein of C57BL/6 mice (10 mice/group). **D,** Reduced extravasation of blue fluorescent shGALC-B16-F10 cells

when co-injected with red fluorescent shNT-B16-F10 cells in the blood circulation of transgenic Tg(kdr:EGFP) zebrafish embryos. Trans-endothelial migration was measured by counting the percentage of cells that migrated across the endothelium of intersomitic vessels in respect to the total number of circulating cells (100-300 cells/experimental point). *Right panels*: Representative images of the trunk of zebrafish embryo showing an extravasating red fluorescent shNT-B16-F10 cell (white arrow) and circulating blue fluorescent shGALC-B16-F10 cells. **E,** *Galc* downregulation inhibits the metastatic activity of B16-F10 cells in zebrafish. Red fluorescent cells were injected (10 embryos per group) into the blood circulation of transgenic Tg(kdr:EGFP) zebrafish embryos. During the next 3 days, red fluorescent metastases in the tail region were quantified by computerized image analysis. Representative images of shNT-B16-F10 and shGALC-B16-F10 metastases are shown. Scale bar: 100 μm. Data are the mean ± SEM, * $P < 0.05$, ** $P < 0.01$.

Figure 5. GALC modulates the tumorigenic activity of human melanoma A2058 cells. **A,** GALC enzymatic activity TLC assay in A2058 cells following gene silencing or upregulation. **B,** An inverse correlation was observed between GALC activity and *Smpd3* gene expression in the different A2058 cell populations. **C-D,** upGALC-A2058 cells show a higher proliferative capacity *in vitro* or when grafted in NOD/Scid mice (9-11 mice/group) whereas GALC down-regulation results in a decreased rate of growth of A2058 cells *in vitro* and *in vivo*. **E,** Immunohistochemical (ICH) analysis of ceramide and SMPD3 immunoreactivity in the tumor grafts generated by the different A2058 cell populations (9-11 tumors/group). Data are the mean ± SEM, * $P < 0.05$, ** $P < 0.01$.

Figure 6. GALC expression correlates with human melanoma progression. **A-B,** RNAscope and immunohistochemical (ICH) analyses show a progressive increase of *GALC* mRNA expression and MITF/tyrosinase immunoreactivity in histological samples from 60 patients at different stages of melanoma progression, including common nevi (CN), dysplastic nevi (DN), melanoma stages I-II (M I-II), III (M III), and IV (M IV). Scale bar: 60 μm. Bonferroni post-test was used to compare all groups after 1-way ANOVA. Statistical significance: * $P < 0.05$, ** $P < 0.01$ *vs* CN. **C,** Spearman rank correlation between *GALC* expression levels and MITF and tyrosinase immunoreactivity as measured in the 60 samples independently of their tumor stage.

Figure 7. SMPD3 and ceramide levels are inversely related to *GALC* expression in human skin melanoma. **A-B,** Immunohistochemical (ICH) analysis of SMPD3 and ceramide immunoreactivity in histological samples from the 60 patients at different stages of melanoma progression analyzed in Figure 6. Scale bar: 60 µm. ** $P < 0.01$ or better *vs* CN. **C,** Spearman rank correlation between *GALC* expression levels and SMPD3 and ceramide immunoreactivity as measured in the 60 samples independently of their tumor stage. *Inset*: correlation of ceramide immunoreactivity data and the *GALC* mRNA/SMPD3 immunoreactivity ratio data.

Figure 1

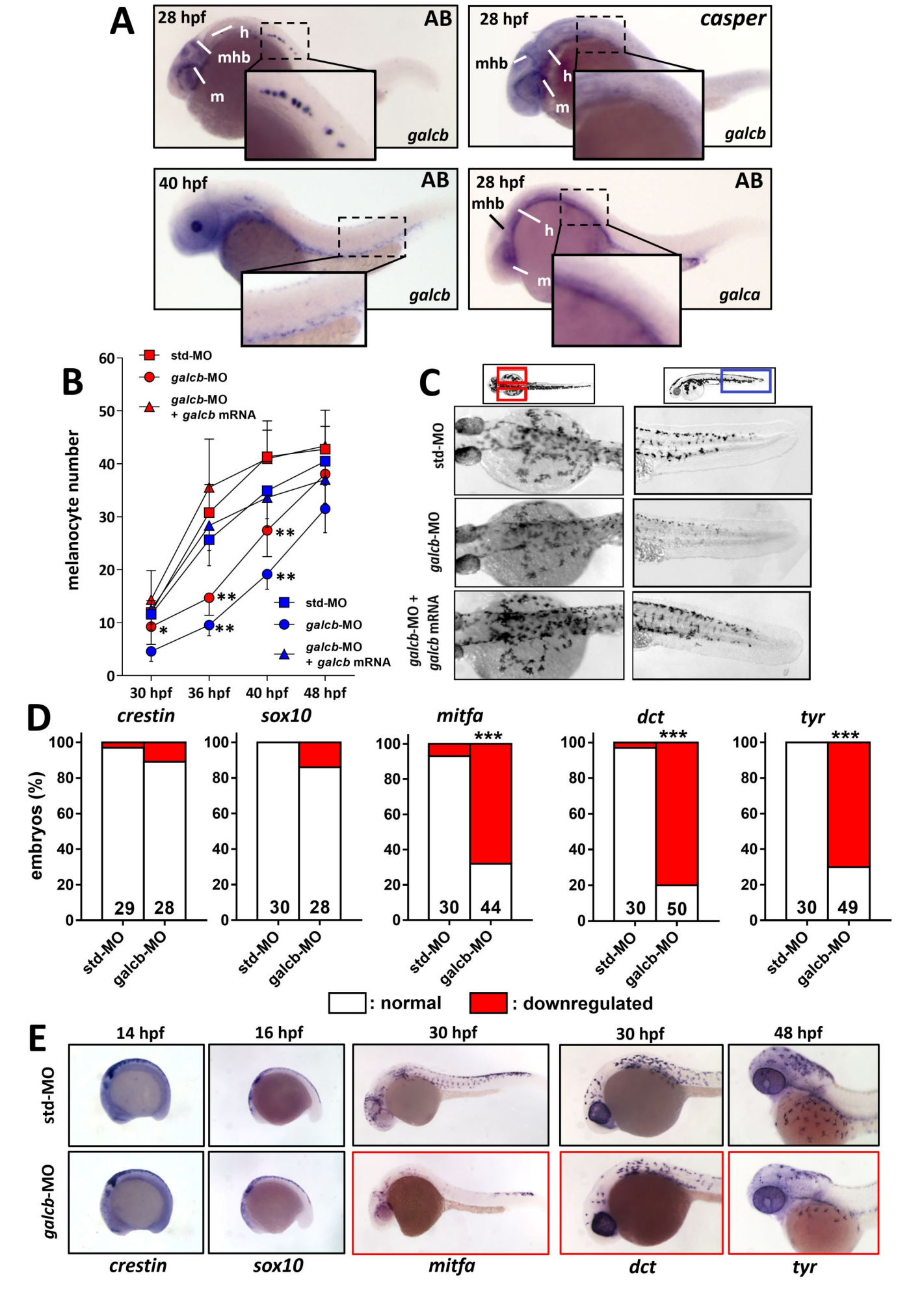
A
28 hpf
AB
h
mhb
m
galcb
28 hpf
casper
mhb
h
m
galcb
40 hpf
AB
galcb
28 hpf
AB
mhb
h
m
galca
B
std-MO
galcb-MO
galcb-MO
+ galcb mRNA
melanocyte number
60
50
40
30
20
10
0
30 hpf
36 hpf
40 hpf
48 hpf
*
**
**
**
**
std-MO
galcb-MO
galcb-MO
+ galcb mRNA
C
std-MO
galcb-MO
galcb-MO +
galcb mRNA
D
crestin
sox10
mitfa
dct
tyr
embryos (%)
100
80
60
40
20
0
***
***
***
29
28
30
28
30
44
30
50
30
49
std-MO
galcb-MO
: normal
: downregulated
E
14 hpf
16 hpf
30 hpf
30 hpf
48 hpf
std-MO
galcb-MO
crestin
sox10
mitfa
dct
tyr

Figure 2

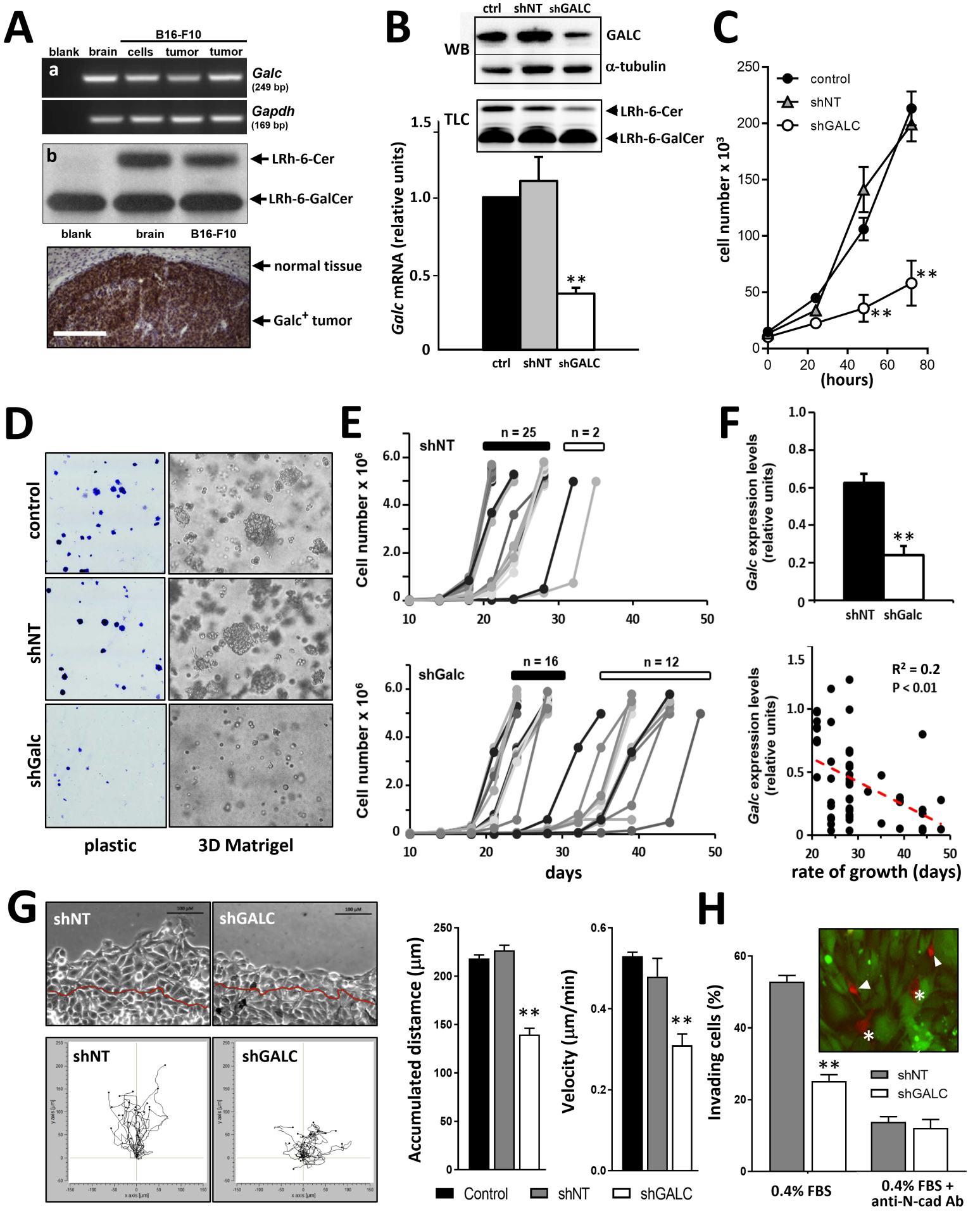
A
B16-F10
blank
brain
cells
tumor
tumor
a
Galc
(249 bp)
Gapdh
(169 bp)
b
LRh-6-Cer
LRh-6-GalCer
blank
brain
B16-F10
normal tissue
Galc+ tumor
B
ctrl
shNT
shGALC
WB
GALC
α-tubulin
TLC
LRh-6-Cer
LRh-6-GalCer
Galc mRNA (relative units)
1.5
1.0
0.5
0
**
ctrl
shNT
shGALC
C
control
shNT
shGALC
cell number x 10³
250
200
150
100
50
0
0
20
40
60
80
(hours)
**
**
D
control
shNT
shGalc
plastic
3D Matrigel
E
shNT
n = 25
n = 2
Cell number x 10⁶
6.0
4.0
2.0
0
10
20
30
40
50
shGalc
n = 16
n = 12
Cell number x 10⁶
6.0
4.0
2.0
0
10
20
30
40
50
days
F
Galc expression levels (relative units)
1.0
0.8
0.6
0.4
0.2
0
**
shNT
shGalc
Galc expression levels (relative units)
1.5
1.0
0.5
0
R² = 0.2
P < 0.01
20
30
40
50
rate of growth (days)
G
shNT
shGALC
shNT
shGALC
Accumulated distamce (µm)
250
200
150
100
50
0
**
Velocity (µm/min)
0.6
0.4
0.2
0.0
**
Control
shNT
shGALC
H
Invading cells (%)
60
40
20
0
**
shNT
shGALC
0.4% FBS
0.4% FBS +
anti-N-cad Ab

Figure 3

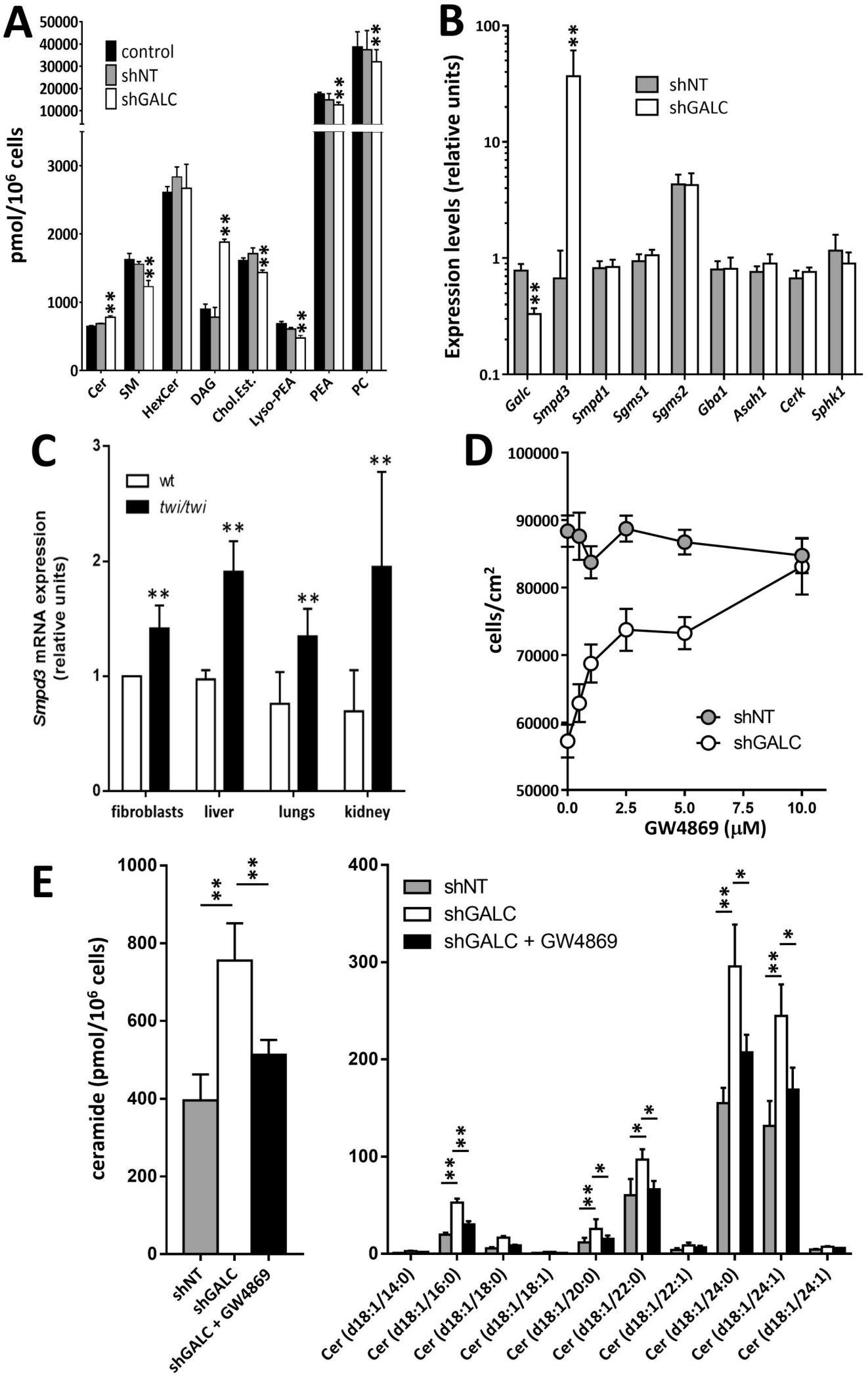
A
pmol/10^6 cells
control
shNT
shGALC
Cer
SM
HexCer
DAG
Chol.Est.
Lyso-PEA
PEA
PC
B
Expression levels (relative units)
shNT
shGALC
Galc
Smpd3
Smpd1
Sgms1
Sgms2
Gba1
Asah1
Cerk
Sphk1
C
Smpd3 mRNA expression (relative units)
wt
twi/twi
fibroblasts
liver
lungs
kidney
D
cells/cm2
shNT
shGALC
GW4869 (μM)
E
ceramide (pmol/10^6 cells)
shNT
shGALC
shGALC + GW4869
Cer (d18:1/14:0)
Cer (d18:1/16:0)
Cer (d18:1/18:0)
Cer (d18:1/18:1)
Cer (d18:1/20:0)
Cer (d18:1/22:0)
Cer (d18:1/22:1)
Cer (d18:1/24:0)
Cer (d18:1/24:1)
Cer (d18:1/24:1)

Figure 4

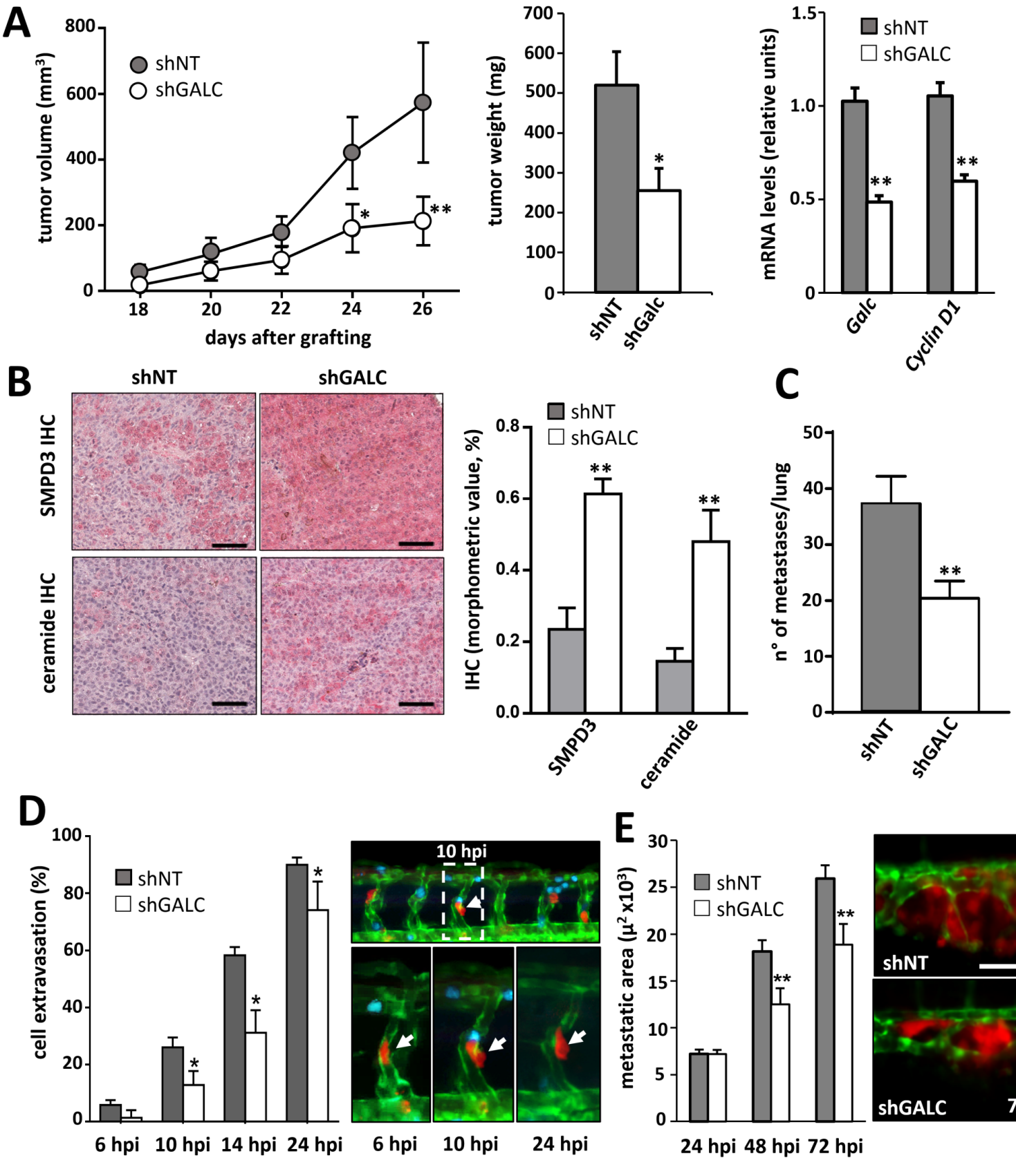
A
tumor volume (mm³)
shNT
shGALC
days after grafting
tumor weight (mg)
shNT
shGalc
mRNA levels (relative units)
Gαlc
Cyclin D1
B
shNT
shGALC
SMPD3 IHC
ceramide IHC
IHC (morphometric value, %)
SMPD3
ceramide
C
n° of metastases/lung
D
cell extravasation (%)
6 hpi
10 hpi
14 hpi
24 hpi
E
metastatic area (μ² x10³)
24 hpi
48 hpi
72 hpi
shNT
shGALC
72 hpi

Figure 5

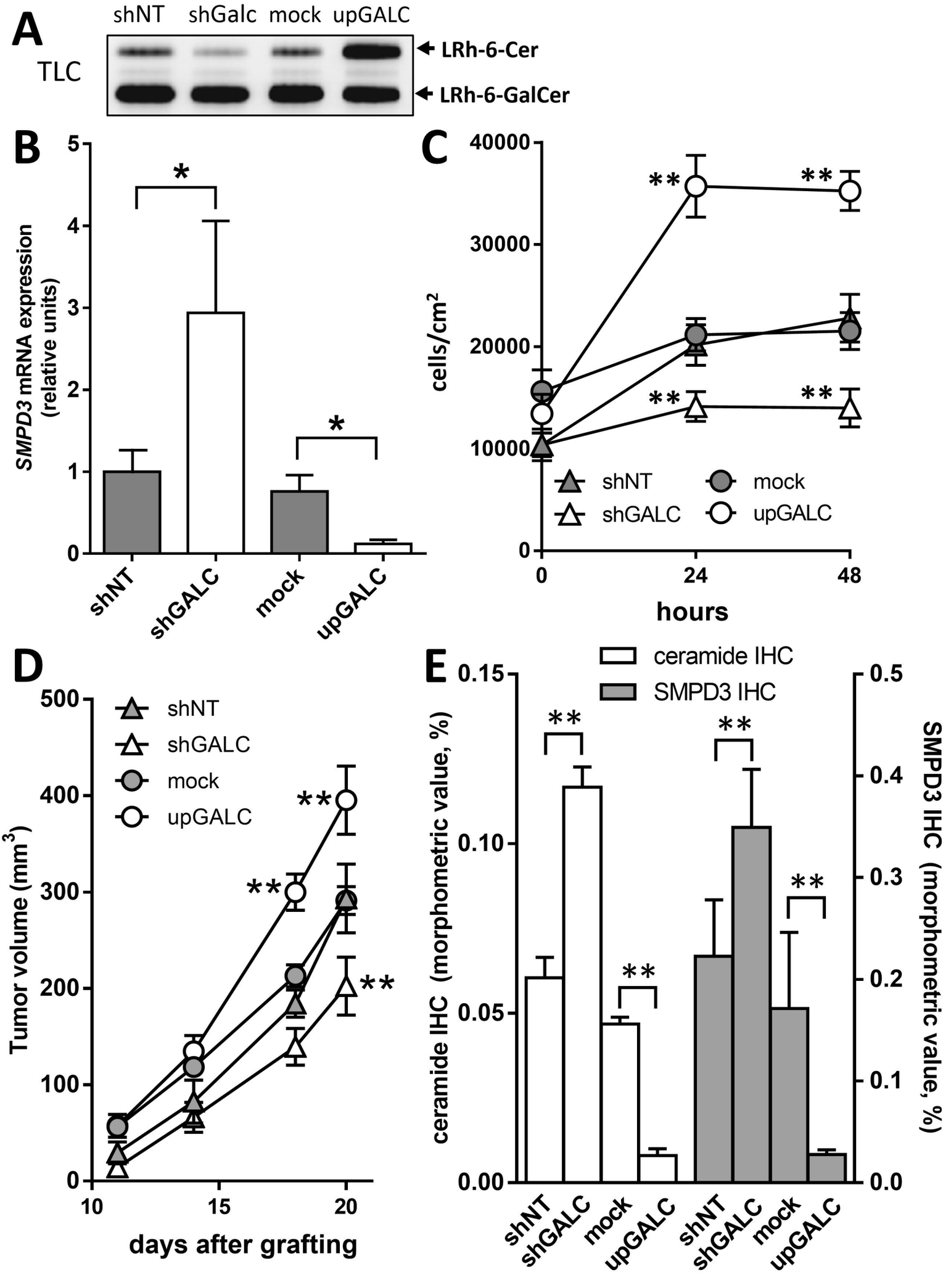
A
shNT
shGalc
mock
upGALC
TLC
LRh-6-Cer
LRh-6-GalCer
B
SMPD3 mRNA expression (relative units)
shNT
shGALC
mock
upGALC
C
cells/cm2
hours
shNT
shGALC
mock
upGALC
D
Tumor volume (mm3)
days after grafting
shNT
shGALC
mock
upGALC
E
ceramide IHC
SMPD3 IHC
ceramide IHC (morphometric value, %)
SMPD3 IHC (morphometric value, %)
shNT
shGALC
mock
upGALC
shNT
shGALC
mock
upGALC

Figure 6

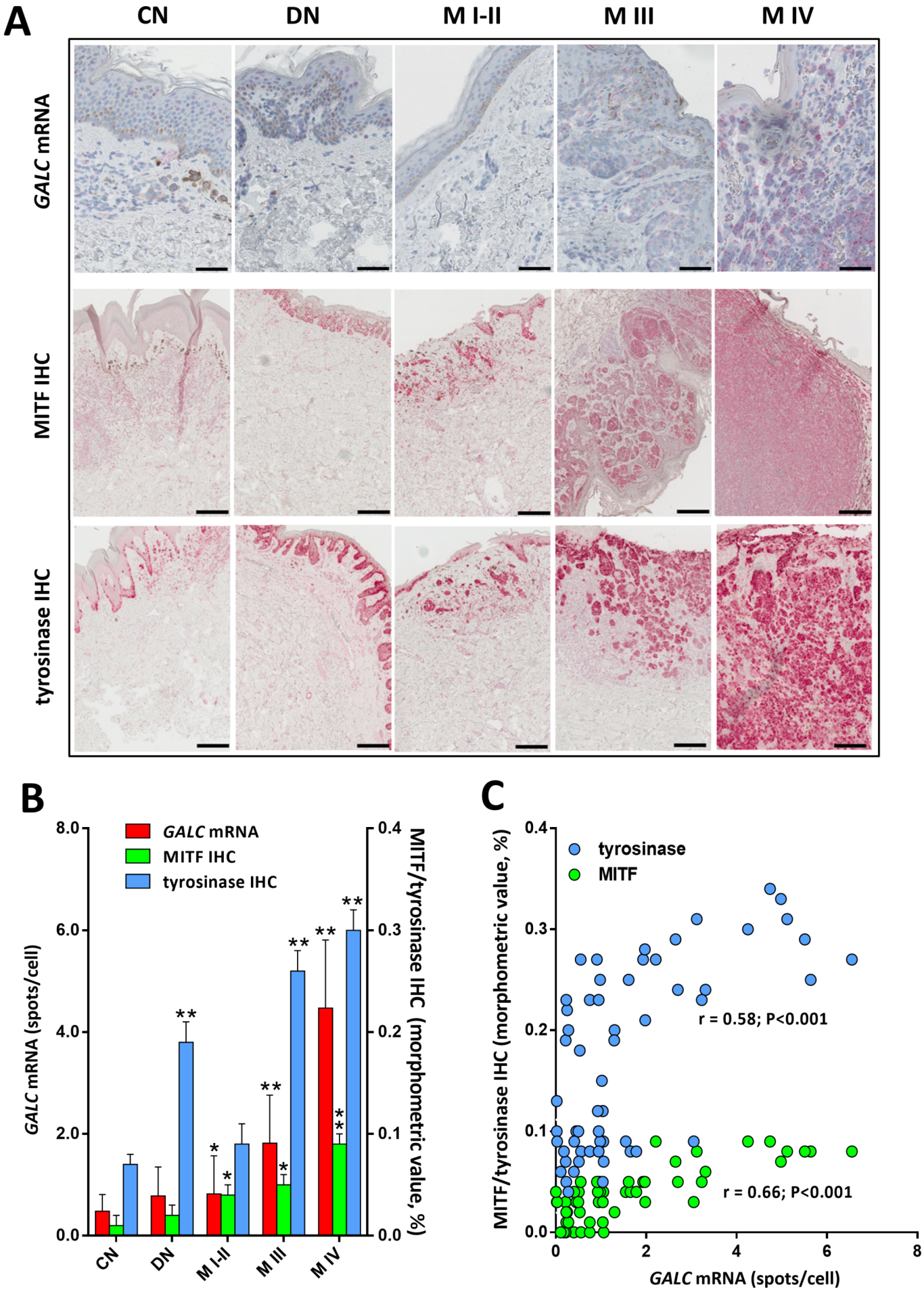
A
CN
DN
M I-II
M III
M IV
GALC mRNA
MITF IHC
tyrosinase IHC
B
GALC mRNA
MITF IHC
tyrosinase IHC
GALC mRNA (spots/cell)
MITF/tyrosinase IHC (morphometric value, %)
8.0
6.0
4.0
2.0
0.0
0.4
0.3
0.2
0.1
0.0
CN
DN
M I-II
M III
M IV
C
tyrosinase
MITF
MITF/tyrosinase IHC (morphometric value, %)
GALC mRNA (spots/cell)
r = 0.58; P<0.001
r = 0.66; P<0.001
0
2
4
6
8

Figure 7

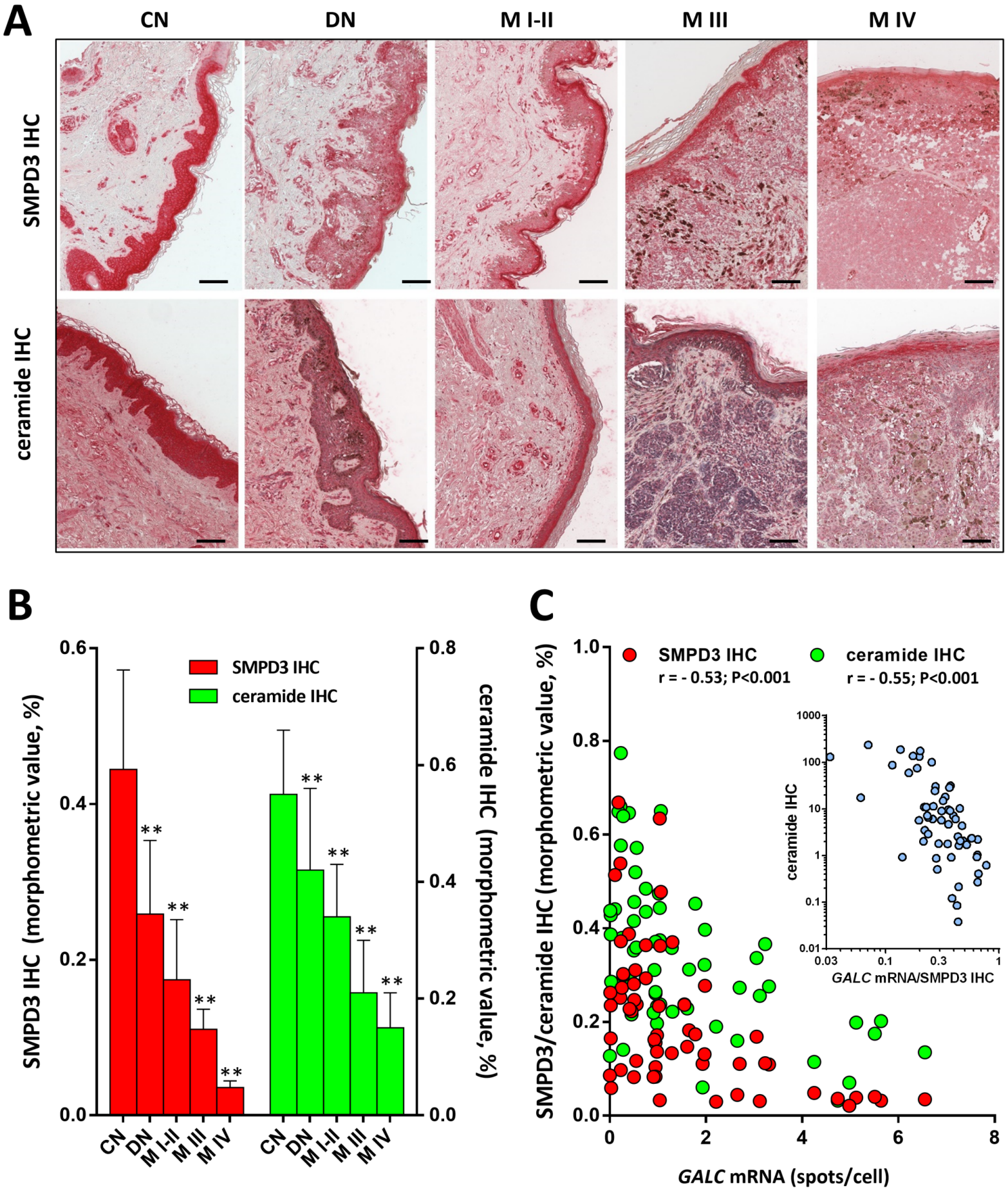
A
CN
DN
M I-II
M III
M IV
SMPD3 IHC
ceramide IHC
B
SMPD3 IHC
ceramide IHC
SMPD3 IHC (morphometric value, %)
ceramide IHC (morphometric value, %)
0.6
0.4
0.2
0.0
0.8
**
CN
DN
M I-II
M III
M IV
C
SMPD3 IHC
r = - 0.53; P<0.001
ceramide IHC
r = - 0.55; P<0.001
SMPD3/ceramide IHC (morphometric value, %)
1.0
0.8
0.6
0.4
0.2
0.0
0
2
4
6
8
GALC mRNA (spots/cell)
ceramide IHC
1000
100
10
1
0.1
0.01
0.03
0.1
0.3
1
GALC mRNA/SMPD3 IHC